

A finite element model of the shoulder: application to the comparison of normal and osteoarthritic joints

P. Büchler^{a,b,*}, N.A. Ramaniraka^{a,b}, L.R. Rakotomanana^c, J.P. Iannotti^d, A. Farron^a

^a Orthopedic Hospital, Lausanne, Switzerland

^b Institute for Biomedical Engineering, Swiss Federal Institute of Technology, 1015 Lausanne, Switzerland

^c Institute of Mathematics, University of Rennes I, Rennes, France

^d The Cleveland Clinic Foundation, Cleveland, OH, USA

Received 10 April 2002; accepted 6 August 2002

Abstract

Objective. The objective of the present study was to develop a numerical model of the shoulder able to quantify the influence of the shape of the humeral head on the stress distribution in the scapula. The subsequent objective was to apply the model to the comparison of the biomechanics of a normal shoulder (free of pathologies) and an osteoarthritic shoulder presenting primary degenerative disease that changes its bone shape.

Design. Since the stability of the glenohumeral joint is mainly provided by soft tissues, the model includes the major rotator cuff muscles in addition to the bones.

Background. No existing numerical model of the shoulder is able to determine the modification of the stress distribution in the scapula due to a change of the shape of the humeral head or to a modification of the glenoid contact shape and orientation.

Methods. The finite element method was used. The model includes the three-dimensional computed tomography-reconstructed bone geometry and three-dimensional rotator cuff muscles. Large sliding contacts between the reconstructed muscles and the bone surfaces, which provide the joint stability, were considered. A non-homogenous constitutive law was used for the bone as well as non-linear hyperelastic laws for the muscles and for the cartilage. Muscles were considered as passive structures. Internal and external rotations of the shoulders were achieved by a displacement of the muscle active during the specific rotation (subscapularis for internal and infrapinatus for external rotation).

Results. The numerical model proposed is able to describe the biomechanics of the shoulder during rotations. The comparison of normal vs. osteoarthritic joints showed a posterior subluxation of the humeral head during external rotation for the osteoarthritic shoulder but no subluxation for the normal shoulder. This leads to important von Mises stress in the posterior part of the glenoid region of the pathologic shoulder while the stress distribution in the normal shoulder is fairly homogeneous.

Conclusion. This study shows that the posterior subluxation observed in clinical situations for osteoarthritic shoulders may also be caused by the altered geometry of the pathological shoulder and not only by a rigidification of the subscapularis muscle as often postulated. This result is only possible with a model including the soft tissues provided stability of the shoulder.

Relevance

One possible cause of the glenoid loosening is the eccentric loading of the glenoid component due to the translation of the humeral head. The proposed model would be a useful tool for designing new shapes for a humeral head prosthesis that optimizes the glenoid loading, the bone stress around the implant, and the bone/implant micromotions in a way that limits the risks of loosening.
© 2002 Elsevier Science Ltd. All rights reserved.

Keywords: Shoulder; Biomechanics; Osteoarthritic; Finite element analysis; Stress distribution

1. Introduction

The glenohumeral joint is the most important joint of the shoulder. It is composed of the humerus and the scapula. Glenohumeral contact occurs between the humeral head, which is almost spherical, and a small shallow depression on the scapula called the glenoid

* Corresponding author.

E-mail address: philippe.buechler@epfl.ch (P. Büchler).

fossa. The poor congruence of the articular surfaces allows the large range of motion of the shoulder but does not contribute to its stability. The soft tissues, especially the rotator cuff muscles, constitute the major stabilizer of the glenohumeral joint [1–3]. Since the bone congruence is poor, the glenohumeral motion is strongly dependent on the shape of the humeral head and on the muscle balance. Altered shapes of the humeral head, in case of osteoarthritis, after prosthetic replacements, or a disease-induced modification of the mechanical properties of the muscles, may induce a modification of the glenohumeral motion, and contact location, and thus may modify the bone stresses in the scapula.

In order to track the behavior of the glenohumeral joint, a numerical model has to include both the exact bone geometry and the stabilizing muscles of the joint. Numerous models of the human shoulder have been proposed. The first models were based on the inverse dynamic theories [4–7] and were used to determine the muscular forces. Models based on the deformable body concept [8–12] were then proposed and used to calculate stress distribution within individual bones of the joint. The most recent models combine both approaches by using the muscular forces obtained with the inverse dynamic theory to calculate the stress with a finite element (FE) model [13,14]. However, none of these models is able to determine the modification of the glenohumeral motion due to a change of the shape of the humeral head, nor the precise location of the contact point on the glenoid surface, which are determinant for the stress distribution in the scapula.

The goal of this study was to develop a three-dimensional (3D) FE model of the shoulder that includes the major rotator cuff muscles. Reconstruction of the muscular tissue allows simultaneous determination of the glenohumeral motion in function of the bone geometry and calculation of the bone stress distribution. The model was then applied to study normal and osteoarthritic (OA) shoulders and results obtained with the numerical model were compared with clinical observations. In case of osteoarthritis, a posterior wear of the glenoid region as well as posterior subluxation of the humeral head are frequently observed. The objective of the model is to reproduce these clinical findings and to show the effects of the OA glenohumeral anatomy on the joint motion and bone stress during internal (IR) and external rotations (ER).

2. Methods

2.1. Data acquisition

Two human fresh frozen cadavers shoulders were used: a normal, without any evidence of pathology and an OA one, with primary degenerative disease that

changed its bone shape and density but without any full thickness tear of rotator cuff tendons. Twelve radio-opaque zirconium beads, 0.5 mm in diameter, were implanted percutaneously in the bone cortex of each shoulder (six in the humerus and six in the scapula). The beads were used to define a coordinate system fixed to each bone. Computed tomography (CT) scans of both shoulders were performed (helical CT, General Electric). Slices 1 mm thick were obtained from the acromion to the middle portion of the humerus. CT provided data about bone geometry and bone density distribution.

The three major rotator cuff muscles (subscapularis, supra and infraspinatus) were included in the model. A careful dissection of both shoulders was performed for this purpose. The insertions of the three muscles on the humerus and the scapula were accurately located. Using a Polhemus 3Space Fastrak Stylus (Polhemus 3Space Fastrak, Colchester, Vermont, USA) [15], the exact insertion and origin of the three muscles were digitized. Four points at the corner of each muscle were recorded to represent the insertions (eight points per muscle). The positions of the zirconium beads were then accurately located and digitized using the Polhemus during the dissection. As the zirconium beads were visible on CT, it was possible to place the muscles in the same coordinate system as the CT images.

2.2. Finite element model reconstruction

The external contour of bone was accurately defined on each CT slice with a digitization error lower than 0.7 mm (2 pixels). The obtained curves were then transferred in the PATRAN software (MacNeal-Schwendler, South Coast Metro, California, USA) and used to reconstruct the 3D geometry of the scapula and of the proximal humerus of both shoulders. The FE mesh of the reconstructed bone was divided into two parts. For both shoulders, the scapula and the spinatus were meshed using 8-node hexahedral volume elements (C3D8) and the humerus was meshed with 4-node rigid surface elements (R3D4). About 11000 3D elements and 800 2D rigid elements were used for each shoulder (Fig. 1). The humerus was meshed with rigid elements in order to limit the size of the model and the calculation time. We have shown that this approximation did not modify the glenohumeral contact region, force or the stress distribution in the scapula [16]. The commercial FE software ABAQUS/standard 5.8-1 (Hibbitt, Karlsson and Sorensen Inc., Pawtucket, Rhode Island, USA) was used for the simulations, and the name of the elements refer to this software.

Custom-made software was designed to read the density from CT slices and to automatically incorporate the non-homogeneous distribution of bone density into the meshes. This software first read all the CT

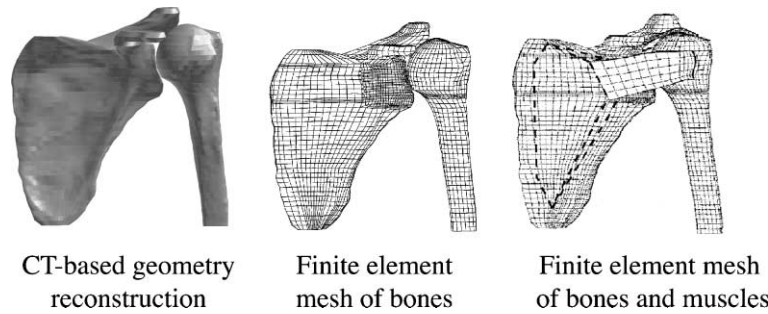


Fig. 1. Major steps of the model reconstruction.

Table 1

Description of the constitutive laws used in the model (I_1 and I_2 are the first and second invariants of the Cauchy–Green tensor)

Element	Type of the law	Mathematical expression	Constants	References
Bone	Linear elastic, non-homogenous	$E(\rho) = E_0(\rho/\rho_0)^2$, $\nu = \nu_0$	$E_0 = 15000$ MPa, $\nu_0 = 0.3$, $\rho_0 = 1.8$ g/cm ³ , ρ : bone density	[36–38]
Muscles	Exponential hyperelastic, incompressible	$W = \alpha \exp[\beta(I_1 - 3)] - \alpha\beta/2(I_2 - 3)$	$\alpha = 0.12$ MPa, $\beta = 1.0$	[20,21,39]
Cartilage	Neo-Hookean hyperelastic, incompressible	$W = C_{10}(I_1 - 3)$ with $C_{10} = E/4(1 + \nu)$	$C_{10} = 1.79$ ($E = 10$ MPa, $\nu = 0.4$)	[40,41]

images, computed a relative density for each node of the mesh and then saved the resulting list in an output file [17]. The mechanical properties of the deformable bone region depend on the square of the apparent density (Table 1). According to this quadratic dependency, a non-homogeneous bone constitutive law was developed [18,19] and implemented in the FE software.

The 3D geometry of the subscapularis, supra and infraspinatus muscles was reconstructed. We considered the muscular insertions on the bone surfaces of the humerus and scapula as defined by the four landmarks defined after dissection. The muscular belly was assumed to be an isoparametric solid between the two insertions surfaces, that winds around the previously reconstructed bone geometry. Three-dimensional muscles were then meshed with about 1200 hexahedral hybrid 3D elements (C3D8H) (Fig. 1). In the present study, only the passive behavior of the muscles was accounted for. The passive stress–strain law applied to the muscles (Table 1) was based on the strain energy function of Veronda [20] that has been recently applied for other joint soft tissue as ligaments and tendons [21,22].

The articular cartilage of the normal shoulder was also reconstructed. The OA shoulder had no cartilage in the region of the glenohumeral contact. For the normal shoulder, the reconstruction was based on the hypothesis that the space observed on the CT images between the humerus and scapula was filled with cartilage. The minimum gap was measured and the 3D cartilage was reconstructed with a constant thickness equal to the half of this distance. The FE mesh of the cartilage was made of 2000 hexahedral hybrid 3D elements (C3D8H). A Neo-Hookean incompressible constitutive law was used for the cartilage (Table 1).

2.3. Loading conditions

The muscles were fixed on the humerus at the insertion sites defined after dissection. The scapular insertions of the muscles were not 3D reconstructed (Fig. 1). The extremity of the scapular side of the muscles had a motion controlled by the boundary conditions (Fig. 2A). These displacements represent the contractions of the muscles. An initial pre-stress (IPS) of 1.5 kPa was introduced in all the muscles by an imposed displacement of the scapular extremity of the muscles in the direction of their insertions sites on the scapula. The additional displacements of the scapular extremity of the muscles were the same as the displacements of the scapula.

The neutral position of the glenohumeral joint (0° of rotation) was defined as the position in which the center of the humeral articular surface faces the center of the glenoid fossa (Fig. 2A). From this neutral position an ER (up to 30°) was achieved by imposing a gradual displacement of the scapular extremity of the infraspinatus muscle. Similarly, an IR (up to 40°) was achieved by imposing a displacement to the scapular extremity of the subscapularis muscle (Fig. 2A). The motions were chosen to be pure rotations. Boundary conditions imposed on the distal extremity of the humerus prevent motions of adduction/abduction and motions of flexion/extension. For the boundary conditions, a coordinate frame was defined at the bottom of the humerus with one axis (e_3) oriented in the direction of the humerus diaphysis and with an other axis (e_1) oriented parallel to the plane of the scapula (Fig. 2C). Flexion/extension were prevented by imposing zero rotation around e_1 ($UR_1 = 0$) and abduction/adduction were prevented by imposing zero rotation around e_2

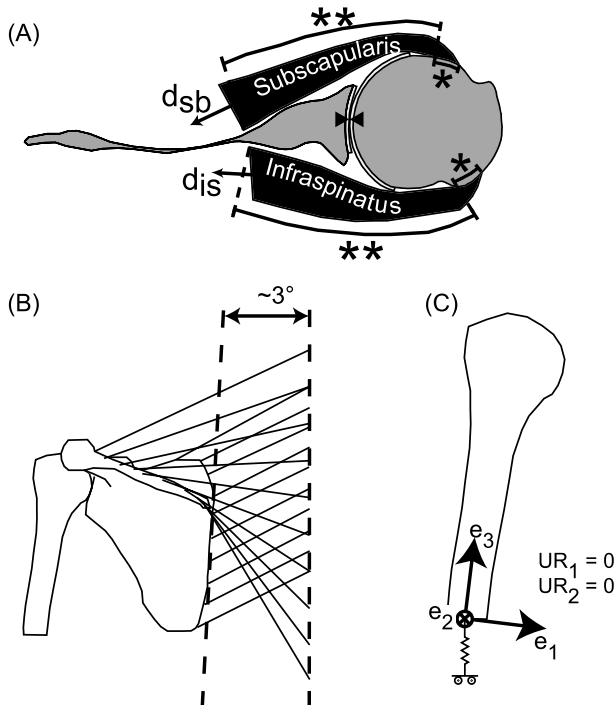


Fig. 2. Boundary conditions on the shoulder. (A) Represents an horizontal slice of the glenohumeral joint. The contacts between the muscles and the bone are divided into two regions; the first region (*) represents the insertion of the muscles on the humerus and the second region (**) represents the bone/muscle large sliding contact. First an IPS was introduced in the muscles by an imposed displacement of the scapular part of the muscles (d_{is} , d_{ss} (not represented) and d_{sb}). The scapular parts of the muscles were then attached to the scapula, except for the muscle active in the simulated rotation. An additional displacement was then imposed to the active muscle (subscapularis for IR and infraspinatus for ER) which generate the rotation. (B) Represents the directions of the stabilizing muscles of the scapula: the trapezius and the rhomboideus are modeled as spring elements. The muscles are inserted on a line representing the spine. The angle between the scapula and the spine is 3° [35]. (C) Describes the boundary conditions imposed on the distal part of the humerus. The spring only limits the vertical translation of the humerus.

($UR_2 = 0$). The angular rotation was measured by the rotation around e_3 . The vertical translation of the humerus was constrained by a vertical spring (SPRINGA, $k = 1000$ N/mm), precluding any significant vertical translation of the humerus (Fig. 2C).

During the rotations, the scapula was not rigidly fixed in the reference frame, but was maintained by 20 spring elements (SPRINGA, $k = 100$ N/mm) simulating the stabilizing muscles of the scapula: the trapezius, the rhomboideus major and the rhomboideus minor (Fig. 2B). The gliding of the scapula on the thorax was also reconstructed by introducing three spring elements (SPRINGA, $k = 100$ N/mm) in the antero-posterior direction.

Glenohumeral contacts and bone–muscles contacts were considered in the model. These contacts were modeled with discontinuous unilateral large sliding laws. The normal contact laws were based on an exponential function. The laws allowed some penetrations of the slave surface nodes into the master surface and considered a contact force with a positive contact distance. These considerations provided a good numerical stability of the model. The law used for the glenohumeral contact allowed more penetrations than the law used for the bone–muscles contacts (Fig. 3A). The Coulomb friction was used for the tangential contact law (Fig. 3B). The coefficient of friction was set to $\mu = 0.001$ for the cartilage–cartilage glenohumeral contact of the normal shoulder and $\mu = 0.1$ for the OA shoulder cortical bone–cortical bone contact (this coefficient was chosen between $\mu = 0.6$, which is the coefficient of friction cortical bone–spongy bone [23], and 0.001). The contacts between bone and muscle were considered without friction (i.e. $\mu = 0$). All contacts were defined between rigid bodies and deformable surfaces except the glenohumeral contact of the normal shoulder that was defined between two deformable bodies.

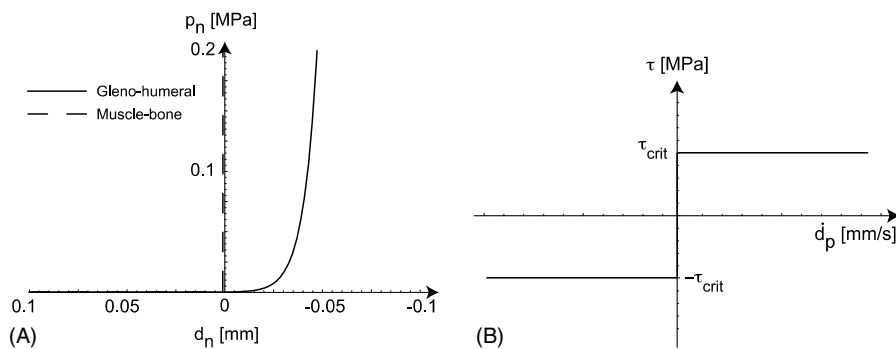


Fig. 3. (A) The normal contact law used for the glenohumeral and bone–muscles large sliding contacts. p_n is the normal contact pressure and d_n is the normal distance between the contacting surfaces. (B) Tangential contact law used for the contacts. τ is the contact shear stress and \dot{d}_p is the parallel sliding velocity. The critical shear stress is related to the contact pressure p_n by the relation: $|\tau_{crit}| = \mu p_n$, with μ the friction coefficient.

3. Results

3.1. Evaluation of the model stability

Parametric studies were conducted to evaluate the robustness of the model. The parameter used to evaluate the glenohumeral motion was the centroid of the contact pressure defined as

$$\vec{G} = \frac{\sum_i P_i \vec{x}_i}{\sum_i P_i}$$

with P_i the contact pressure at the node i and x_i the position of the node i . This parameter synthesizes all the results since the bone stress distribution in the scapula is modified only if the glenohumeral contact region moves. The case of reference was defined with $k = 1000$ N/mm for the spring on the distal humerus and with an IPS of 1.5 kPa on all the muscles. From this reference, the displacement of the center of contact and the value of the total force transmitted by the glenohumeral contact were compared for the maximal angle of rotations. The displacements of the centroid of the contact were mea-

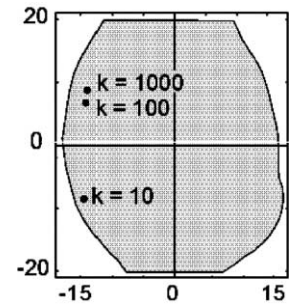
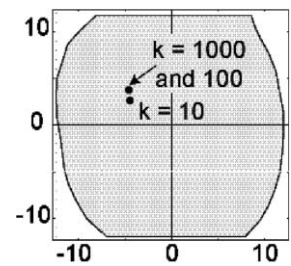
sured in both horizontal and vertical direction on the glenoid surface (Table 2).

Three different stiffnesses of the spring on the distal humerus ($k = 10, 100, 1000$ N/mm) were tested for internal and external rotations of the normal shoulder (Table 2). The results showed that the modification of the rigidity only changed the vertical location of the glenohumeral contact region. The horizontal displacements of the contact region were less than 0.8 mm. For $k = 10$, the contact was located in the inferior part of the glenoid fossa for maximal rotations with the OA shoulder. The vertical translation of the contact region modified the contact forces, but for $k \geq 100$ the contact force did not vary significantly.

The second parameter studied was the effect of the initial muscular pre-stress. Three different pre-stress were studied (IPS = 0, 1.5, 3 kPa). A pre-stress of 3 kPa represents a force of about 2 N in the subscapularis and infraspinatus muscles, which is more than 10% of the maximal force during the rotation of the normal shoulder. Results are given in Table 2. The IPS did not modify the glenohumeral contact location on the glenoid fossa.

Table 2
Effect of the rigidity of the spring on the distal humerus and of the initial muscular pre-stresses on the glenohumeral contact location and forces

Rigidity (N/mm)	IPS (kPa)	40° RI			30° RE		
		Disp.x (mm)	Disp.y (mm)	Contact force (N)	Disp.x (mm)	Disp.y (mm)	Contact force (N)
<i>Normal shoulder</i>							
10	1.5	0	-0.6	31.7	-0.1	-1.1	32.1
100	1.5	0	0	31.6	0	0	32.0
1000	1.5	0	0	31.5	0	0	31.9
1000	0	-0.3	0.1	27.3	-0.2	-0.4	26.8
1000	1.5	0	0	31.5	0	0	31.9
1000	3	0.2	0.1	35.3	0.1	-0.4	35.3
<i>OA shoulder</i>							
10	1.5	-0.2	-17.7	32.5	-0.5	-17.2	66.2
100	1.5	-0.1	-1.3	38.7	-0.1	-2.1	75.5
1000	1.5	0	0	41.2	0	0	77.4
1000	0	0.4	-1.1	30.5	-0.3	-0.2	70.2
1000	1.5	0	0	41.2	0	0	77.4
1000	3	-0.2	0.6	47.3	0.8	0.8	87.1



Disp.x and Disp.y are the displacements of the centroid of the contact pressure relative to the reference case ($k = 1000$, pre-stress 1.5) along the horizontal and vertical axes respectively. The figures on the right represent an example of the centroid of the contact pressure on the glenoid fossa for the normal and OA shoulder at 30° external rotation. The x-axis is horizontal and the y-axis is vertical.

The only modification observed was the expected increase of the normal contact forces for higher pre-stress.

The effect of the stiffness of the spring elements stabilizing the scapula was evaluated. No modification of the glenohumeral contact position and contact forces was observed for stiffness of $k = 10, 100$ and 1000 N/mm . Finally, the effect of the friction coefficient of the OA glenohumeral contact was investigated. Results showed a posterior translation 3 mm less important for $\mu = 0.01$ compared to the values for $\mu = 0.1$.

3.2. Application to normal and osteoarthritis shoulders

Biomechanical results obtained with the model for a normal and an OA shoulder are presented. The model of the normal shoulder was used as the reference situation and results achieved with the OA model were compared to this reference case.

The glenoid contact pressure was calculated for normal and OA shoulders during progressive external and internal rotations (Fig. 4). During rotations, the contact zone remained centered in the glenoid fossa for the normal shoulder. For the OA shoulder, a posterior translation of the contact region was observed during ER. This posterior translation was associated to an increase of the contact pressure. At maximal ER, the contact pressure was about two times higher in the OA shoulder than in the normal one. No significant translation of the contact region was observed during IR for the OA shoulder. The total force transmitted through the glenohumeral contact is also higher with the OA shoulder (Table 3). For ER, the normal contact force is about 2.5 times higher for the OA shoulder than for the normal one. Table 3 shows that shear contact forces are equivalent to the normal contact force divided by the friction coefficient. This result indicates that all glenohumeral contacts are sliding for maximal angles of rotations.

The von Mises shear stresses are represented for the maximal angle of external and internal rotations (Fig. 5) for both shoulders in a horizontal slice of the scapula. The stress in the glenoid was very important in the posterior region during ER for the OA shoulder. In this

Table 3
Normal and shear contact forces

	Normal shoulder		OA shoulder	
	30° RE	40° RI	30° RE	40° RI
Contact normal force	31.9	31.5	77.4	41.2
Contact shear force	3.2×10^{-2}	3.2×10^{-2}	7.8	4.1

region, the von Mises maximal values were about three times higher in the OA glenoid at 30° ER than in the normal shoulder.

The forces developed in the subscapularis and infraspinatus muscles during rotations are shown in the Fig. 6. The force calculated in the supraspinatus muscle was not important during the rotations (not presented). The forces calculated with the OA model were higher than the forces calculated for the normal shoulder. The difference between the forces in the normal and OA shoulder was more important when the muscle was active (infraspinatus muscle for ER and in the subscapularis muscle for IR). The maximum difference of the muscular force between the two shoulders was at 30° ER. In this case, the force in the infraspinatus muscle was more than four times higher for the OA shoulder than for the normal one.

4. Discussion

The purpose of this study was to develop a numerical model of the shoulder that is able to quantify the influence of the geometry of the humeral head on the bone stress distribution in the scapula. The presented FE model allows the simultaneous calculation of motions and internal forces such as contact pressure, bone stress and muscle forces. Since soft tissues play a major role in the shoulder motion they were included in the biomechanical model. As illustration, the model was used to evaluate the alteration of the bone morphology due to osteoarthritis.

Currently available FE models of the shoulder usually deal either with (i) rigid body systems, in which forces and moments are related to the rigid body motions (translations and rotations) through the Newton's

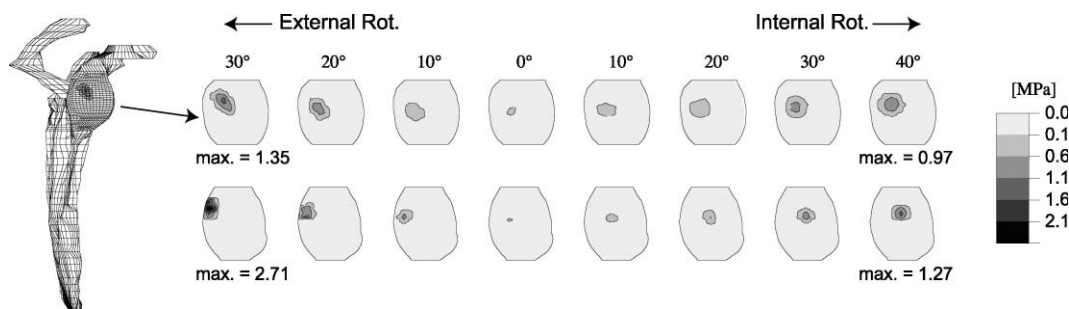


Fig. 4. Contact pressure on the glenoid fossa during internal and external rotations for normal (top) and OA (bottom) shoulders.

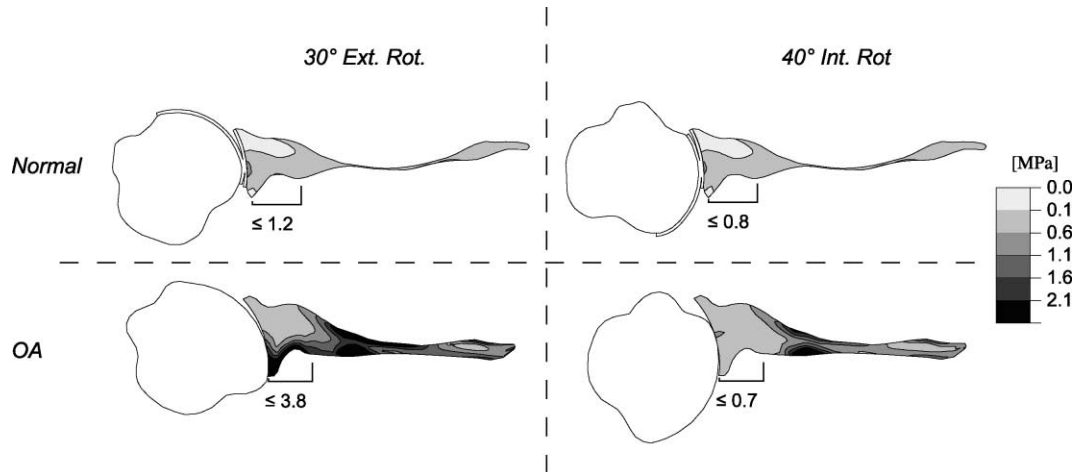


Fig. 5. Distribution of von Mises stress in the scapula for the normal and for the OA shoulder at 40° IR and 30° ER.

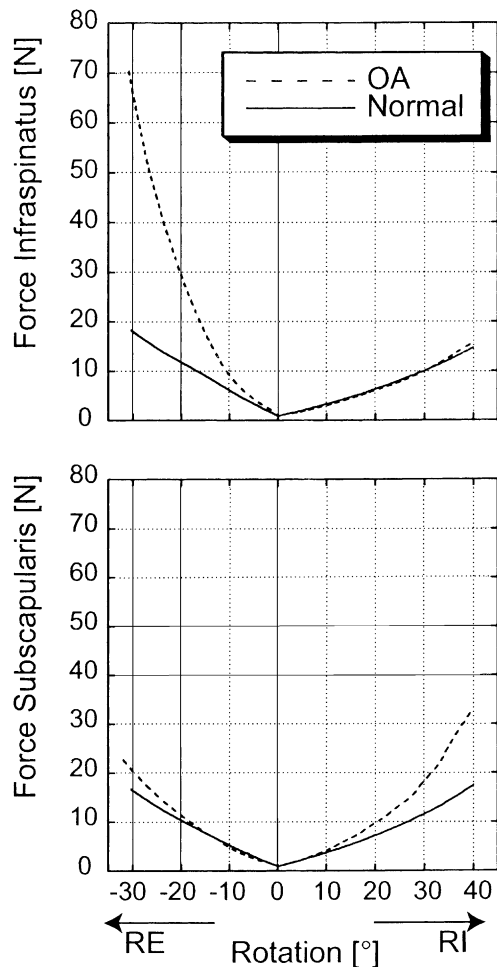


Fig. 6. Force developed in the infraspinatus and subscapularis muscles during rotations for the normal and OA shoulders.

laws of mechanics [4–7] or with (ii) deformable body systems [8–14]. Rigid body models provide useful but coarse approximation of the joint interface behavior. Existing deformable body models do not consider the

joint motion and are submitted to *a priori* calculated external loads representing an approximation of the unknown contact force of the humeral head and muscle forces.

In the present glenohumeral joint model, all the above mentioned limitations were overcome. The 3D reconstruction of muscle was deemed necessary with regard to the overall stability of the model. Indeed, a preliminary version of the present model, which used (non-)linear springs to model the muscles, did not allow simulation of either ER or IR due to its numerical instability. Providing an accurate 3D-muscle reconstruction, the model was able to describe large displacements of the joints together with finite rotations of bones, from which the rigid kinematics could be easily extracted. Bone constitutive laws include not only its elasticity but also the accurate non-homogeneous distribution of bone density. This feature is essential to determine the precise bone stress distribution and cannot be neglected if the future application of model is to analyze the anchorage of orthopedic prostheses. Bone stresses expressed as hydrostatic pressure and von Mises shear stress could be evaluated during external and internal rotations of the humerus. The knowledge of these basic stresses is essential to simulate bone remodeling and then provide some biomechanical insights to explain bone growth of the glenoid and the humerus.

As for all numerical models, the boundary conditions are a difficult task. In the case of the shoulder, it is virtually impossible to reproduce exactly the real boundary conditions with all the muscles acting together to provide the shoulder stability and motion. For this reason, the boundary conditions were chosen to reproduce pure rotations. Obviously, the conditions imposed on the distal part of the humerus are a limitation of the model. These two boundary conditions ($UR_1 = 0$, $UR_2 = 0$) replace the effect of non-modeled part of the shoulder like the weight of the arm, omitted muscles,

and the omitted articular capsule. The two boundary conditions avoid motions of abduction and flexion during the rotation. Different stiffnesses of the spring retaining the distal humerus have been tested (Table 2). The principal effect of the spring is to limit the vertical translation of the humerus. The horizontal displacement is not affected with translation lower than 0.8 mm. For low values of the rigidity, the vertical translation becomes important in the OA shoulder, leading to unrealistic glenohumeral contacts in the inferior extremity of the glenoid surface. For this reason, a rigidity of 1000 N/mm has been chosen for the humeral distal spring for both shoulders. A property difficult to evaluate is the cortical bone/cortical bone coefficient of friction. For the OA shoulder, a value of $\mu = 0.1$ was used in this study and thought to be reasonable based on the comparison with other friction couples. The effect of variation of this value was also investigated and results showed the same behavior with $\mu = 0.01$ than with $\mu = 0.1$. Posterior translation during ER and a central glenohumeral contact during IR were observed. This result shows that the friction has a marginal influence on the amplitude of the antero-posterior translation of the contact region observed in the OA shoulder.

Another shortcoming of the model is the limited number of muscles considered. Clearly, internal and external rotations of the shoulder are generated by more than one single active muscle and stabilized by more than two muscles. Nevertheless the modeled muscles are the most important for the glenohumeral stability. It has been shown that the infraspinatus is the principal external rotator of the humerus and accounts for about 60% of ER force [7,24]. In the same way, the subscapularis is the primary internal rotator accounting for about 50% of the IR force [7]. Moreover, [25] showed that the passive subscapularis muscle tension was the primary anterior stabilizer at 0° of abduction. Posterior stability is also provided by passive muscle tension. Both the supraspinatus and the infraspinatus/teres minor are important posterior stabilizers of the shoulder [26–28]. Our results showed that the initial muscular pre-stresses did not influence the glenohumeral contact location. This result led to the same stress distribution pattern in the scapula for the different values of IPSs. Thus, the choice of the IPS is not determinant on the results of the model. This results also means that the exact values of the material parameters used in the muscle law are not crucial for the general model behavior. The most important factor is the general mechanism of stabilization itself with the bone–muscles contacts.

The shoulders used to develop the model were representative of normal and OA group of shoulders. All OA shoulders are not identical, but the general modifications due to the primary degenerative disease observed on the chosen shoulder are typical of OA shoulders. Posterior wear of the glenoid surface [29,30] flatten hu-

meral head and glenoid surface [30] and modification of the retroversion [31,32] are typical characteristics of OA anatomy. In the same way the normal shoulder chosen has the characteristics of healthy shoulders. For this reason, the results obtained with the model are comparable to general clinical findings.

Correlations exist between the results obtained with the numerical model of normal and OA shoulders and clinical observations. The first parallel concerns the posterior translation of the glenohumeral contact calculated for the OA shoulder. This observation corresponds to the posterior humeral head subluxation frequently observed in primary degenerative disease [29]. The von Mises stress distribution indicates also a strong correlation with clinical observations. Regions of high von Mises stress calculated with the model correspond to regions of glenoid wear and bone erosion [29,30]. Finally, the high forces calculated in the active muscle during motion of the OA shoulder are an indication of the limited range of motion observed for OA shoulders [29].

Muscular forces as well as total contact forces calculated with the model were low compared to values found in the literature [4,6,7,33]. The difference may be explained by the different motions considered. In this literature, forces correspond to motion of abduction or to isometric testing. In this study, forces correspond to rotations that require lower forces than abduction. Moreover, rotations considered here were passive in the sense that no force were imposed against the motion.

The present model allowed us to highlight the major biomechanical differences existing between normal and OA shoulders. These differences were due to the alteration of the articular geometry and bone density distribution in the OA shoulder. Results showed that when a shoulder has an OA geometry, the stress in the posterior part of the scapula is important. This induces an increase of the bone remodeling and to the growth of the glenoid surface. The OA geometry leads to an amplification of the pre-existing alteration of the bone geometry. Another important results is that the posterior subluxation observed in this study is not caused by a tight anterior soft tissues as proposed by Matsen et al. [34], since all the muscles have exactly the same properties in the model. This result shows that the posterior subluxation may be explained by the pathological shape of the joint and not only by tight soft tissues. More investigations have to be conducted in order to determine the relative importance of the soft tissues and of the bone shape on the shoulder subluxation.

Our results may have important clinical implications in prosthetic arthroplasty. We found that alteration of the humeral head geometry may greatly influence the contact pressure and stress distribution in the glenoid. A more anatomical humeral head prosthesis could decrease eccentric glenoid loading and consecutively

glenoid stress. Further studies will be necessary to support this hypothesis. A model including total shoulder prostheses is under development to analyze the influence of prosthetic design on bone stress, distribution and micromotions at interfaces (bone–cement–implant). This model could provide valuable information in total shoulder prostheses design.

5. Conclusions

A 3D numerical model of the shoulder has been developed. Application of the model demonstrated significant differences in the biomechanics of the normal and OA shoulders. Results obtained with the model were in agreement with clinical observations on OA shoulders. In this study the biomechanical difference was only caused by the alteration of the bone geometry since the mechanical properties of the soft tissues were identical for the two shoulders. As most of the biomechanical researches to date have used only normal shoulders to define its biomechanics, one should be careful when applying those conclusions to pathological shoulders.

Acknowledgement

This research program is supported by the Swiss National Science Foundation #3200-051148.

References

- [1] Bassett RW, Browne AO, Morrey BF, An KN. Glenohumeral muscle force and moment mechanics in a position of shoulder instability. *J Biomech* 1990;23:405–15.
- [2] Blasler RB, Guldberg RE, Rothman ED. Anterior shoulder stability: contributions of rotator cuff forces and the capsular ligaments in the cadaver model. *J Shoulder Elbow Surg* 1992;1:140–50.
- [3] Cain PR, Mitschler T, Fu FH, Lee SK. Anterior stability of the glenohumeral joint: a dynamic model. *Am J Sports Med* 1987;15.
- [4] van der Helm FC. Analysis of the kinematic and dynamic behavior of the shoulder mechanism. *J Biomech* 1994;27:527–50.
- [5] van der Helm FC. A finite element musculoskeletal model of the shoulder mechanism. *J Biomech* 1994;27:551–69.
- [6] Karlsson D, Peterson B. Towards a model for force predictions in the human shoulder. *J Biomech* 1992;25:189–99.
- [7] Hughes RE, An KN. Force analysis of rotator cuff muscles. *Clin Orthop* 1996;75–83.
- [8] Baréa C, Hobatho MC, Darmana R, Mansat P, Mansat M. Three dimensional finite element modelling of normal and implanted glenoid: validations and simulations. In: *Proceedings of the 11th Conference of the ESB, 1998, Toulouse, France; 1998*. p. 27.
- [9] Friedman RJ, LaBerge M, Dooley RL, O'Hara AL. Finite element modeling of the glenoid component: effect of design parameters on stress distribution. *J Shoulder Elbow Surg* 1992;1:261–70.
- [10] Lacroix D, Prendergast PJ. Stress analysis of glenoid component designs for shoulder arthroplasty. *Proc Inst Mech Eng* 1997;211:467–74.
- [11] Orr TE, Carter DR, Schurman DJ. Stress analyses of glenoid component designs. *Clin Orthop* 1988;217–24.
- [12] Stone KD, Grabowski JJ, Cofield RH, Morrey BF, An KN. Stress analyses of glenoid components in total shoulder arthroplasty. *J Shoulder Elbow Surg* 1999;8:151–8.
- [13] Murphy LA, Prendergast PJ, Resch H. Structural analysis of an offset-keel design glenoid component compared with a center-keel design. *J Shoulder Elbow Surg* 2001;10:568–79.
- [14] Lacroix D, Murphy LA, Prendergast PJ. Three-dimensional finite element analysis of glenoid replacement prostheses: a comparison of keeled and pegged anchorage systems. *J Biomech Eng* 2000;122:430–6.
- [15] Karduna AR, Williams GR, Williams JL, Iannotti JP. Kinematics of the glenohumeral joint: influences of muscle forces, ligamentous constraints, and articular geometry. *J Orthop Res* 1996;14:986–93.
- [16] Büchler P, Rakotomanana LR, Farron A. Virtual power based algorithm for decoupling large motions from infinitesimal strains: application to shoulder joint biomechanics. *Comp. Meth. Biomech. Biomed. Eng.*, in press.
- [17] Terrier A. Adaptation of bone to mechanical stress: theoretical model, experimental identification and orthopaedic applications. Lausanne: EPFL; 1999.
- [18] Terrier A, Rakotomanana L, Ramaniraka N, Leyvraz PF. Adaptation models of anisotropic bone. *Comput Meth Biomech Biomed Eng* 1997;1:47–59.
- [19] Rakotomanana LR, Terrier A, Ramaniraka NA, Leyvraz PF. Anchorage of orthopaedic prostheses: influence of bone properties and bone–implant mechanics. In: Pedersen P, Bendsoe M, editors. *Synthesis in bio solid mechanics*. Dordrecht: Kluwer Academic Publishers; 1999. p. 55–66.
- [20] Veronda DR, Westmann RA. Mechanical characterization of skin-finite deformations. *J Biomech* 1970;3:111–24.
- [21] Pioletti DP, Rakotomanana LR, Benvenuti JF, Leyvraz PF. Viscoelastic constitutive law in large deformations: application to human knee ligaments and tendons. *J Biomech* 1998;31:753–7.
- [22] Pioletti DP, Rakotomanana LR, Leyvraz PF. Strain rate effect on the mechanical behavior of the anterior cruciate ligament–bone complex. *Med Eng Phys* 1999;21:95–100.
- [23] Fitzpatrick D, Ahn P, Brown T, Poggio R. Friction coefficients of porous tantalum and cancellous & cortical bone. In: *Proceedings of the 21st Annual American Society for Biomechanics*. Clemson; 1997.
- [24] Colachis Jr SC, Strohm BR, Brechner VL. Effects of axillary nerve block on muscle force in the upper extremity. *Arch Phys Med Rehabil* 1969;50:647–54.
- [25] Turkel SJ, Panio MW, Marshall JL, Girgis FG. Stabilizing mechanisms preventing anterior dislocation of the glenohumeral joint. *J Bone Joint Surg [Am]* 1981;63:1208–17.
- [26] Ovesen J, Nielsen S. Posterior instability of the shoulder. A cadaver study. *Acta Orthop Scand* 1986;57:436–9.
- [27] Ovesen J, Nielsen S. Anterior and posterior shoulder instability. A cadaver study. *Acta Orthop Scand* 1986;57:324–7.
- [28] Ovesen J, Sojbjerg JO. Posterior shoulder dislocation. Muscle and capsular lesions in cadaver experiments. *Acta Orthop Scand* 1986;57:535–6.
- [29] Matsen FAI, Rockwood CA, Wirth MA, Lippitt SB. Glenohumeral arthritis and its management. In: Rockwood CA, Matsen FAI, editors. *The shoulder*. 2nd ed. Philadelphia: W.B. Saunders Company; 1998. p. 840–964.
- [30] Cofield RH. Degenerative and arthritic problems of the glenohumeral joint. In: Rockwood CA, Matsen FAI, editors. *The shoulder*. Philadelphia: W.B. Saunders Company; 1990. p. 678–749.

- [31] Mullaji AB, Beddow FH, Lamb GH. CT measurement of glenoid erosion in arthritis. *J Bone Joint Surg Br* 1994;76:384–8.
- [32] Friedman RJ. Glenohumeral translation after total shoulder. *J Shoulder Elbow Surg* 1992;1:312–6.
- [33] Anglin C, Wyss UP, Pichora DR. Glenohumeral contact forces. *Proc Inst Mech Eng [H]* 2000;214:637–44.
- [34] Matsen FAI, Lippitt SB, Sidles JA, Harrymann DTI. Practical evaluation and management of the shoulder. Philadelphia: WB Saunders; 1994.
- [35] Matsen FAI, Rockwood CA, Wirth MA, Lippitt SB. Biomechanics of the shoulder. In: Matsen FAI, editor. *The shoulder*. 2nd ed. Philadelphia: W.B. Saunders Company; 1990. p. 233–76.
- [36] Hayes WC. Biomechanics of cortical and tubercular bone: implications for assessment of fracture risk. In: Hayes VCMaWC editor. *Basic orthopaedic biomechanics*. New York: Raven Press; 1991. p. 93–142.
- [37] Reilly DT, Burstein AH, Frankel VH. The elastic modulus for bone. *J Biomech* 1974;7:271–5.
- [38] Rice JC, Cowin SC, Bowman JA. On the dependence of the elasticity and strength of cancellous bone on apparent density. *J Biomech* 1988;21:155–68.
- [39] Pioletti DP, Rakotomanana LR, Leyvraz PF. Strain rate effect on the mechanical behavior of the anterior cruciate ligament–bone complex [In Process Citation]. *Med Eng Phys* 1999;21:95–100.
- [40] Benvenuti JF. *Modélisation tridimensionnelle du genou humain*. Lausanne: Swiss Federal Institute of Technology; 1998.
- [41] Kempson GE. Mechanical properties of articular cartilage. In: Freeman MAR, editor. *Adult articular cartilage*. Kent: Pitman medical; 1979. p. 333–414.